Journal Title
XX(X):2–18

DOI: 10.1177/ToBeAssigned
www.sagepub.com/
SAGE

Wall pressure fluctuations induced by a single stream jet over a semi-finite plate

Stefano Meloni[1], Jack L.T. Lawrence[2], Anderson R. Proença[2], Rod H. Self[2] and Roberto Camussi[1]

Abstract

This work provides an experimental investigation into the interaction between a jet flow and a semi-finite plate parallel to the jet. Wall pressure fluctuations have been measured in a high compressible subsonic regime and for different distances between the jet and the plate trailing edge. The experiment has been carried out in the ISVR anechoic Doak Laboratory at the University of Southampton, using wall pressure transducers flush mounted on the plate surface. Signals were acquired in the stream-wise direction along the jet centreline and in the span-wise direction in a region close to the trailing edge. The radial position of the flat plate was fixed very close to the jet axis to simulate a realistic jet–wing configuration. The plate was moved axially in order to investigate four different jet-trailing edge distances and to include measurements upstream of the nozzle exhaust. The acquired database was analyzed in both the frequency and the time domains providing an extensive statistical characterization in terms of spectral uni– and multi–variate quantities as well as high order statistical moments. A wavelet analysis was performed as well to investigate the time evolution of the wall pressure events.

Keywords

Jet noise, Installation effects , Wall pressure fluctuations

Introduction

The reduction of aircraft noise and fuel consumption has become a key issue for manufacturers in the design of modern aicraft engines. In order to pinpoint a compromise between thrust and fuel consumption, the current tendency is to increase the engine bypass ratio, a solution that, as an indirect benefit, leads to a reduction of the overall noise (1) due to the lower exhaust velocity. The drawback of this configuration is the very large size of the nacelle diameter, which results in the engine being placed very close to the wing in order to maintain the same ground clearance. Such a closely-coupled architecture leads to a stronger interaction between the exhaust flow and the wing as well as a modification of the jet noise generation and propagation mechanisms. These effects are no longer predictable using consolidated models developed for isolated jets. For these reasons, many experimental and numerical studies have been carried out in the last few years to investigate installation noise (2; 3; 4; 5; 6; 7). Studies on simplified jet-flat plate configurations remain important to provide fundamental physical understandings both from the aerodynamic (8; 9; 10; 11) and the acoustic standpoint. To this extent, the shielding/scattering effect of the airframe surface have been investigated by (12; 13) whereas near-field and far-field noise generated by a jet installed close to a semi-finite plate has been analyzed by Lawrence et al. (14).

Wall pressure fluctuations induced by the jet over an infinite flat plate have been extensively investigated in (8; 15; 16; 17; 18) for the prediction of the vibro-acoustic response of the aircraft surfaces.

The statistical analysis of jet-induced wall pressure fluctuations is also the subject of the present work where the stream issued by a highly compressible subsonic jet flow convects across a semi-finite plate. The main novelty proposed therein is the parametric study carried out in terms of the axial distance between the nozzle exit plane and the trailing edge, an

[1] Department of Engineering, University of RomaTre, Rome,00146, RM, Italy
[2]Institute of Sound and Vibration Research, University of Southampton, Southampton, SO17 1BJ, Hampshire,UK

Corresponding author:
Stefano Meloni,Department of Engineering, University of RomaTre, Rome,00146, RM , Italy
Email: stefano.meloni@uniroma3.it

issue that has never been investigated before even though it is of interest for realistic jet-wing installation architectures.

The reported investigation was performed under static ambient flow conditions at a jet Mach number $M = 0.75$. The plate was positioned at $H/D = 0.67$, where H is the radial distance between the plate surface and the jet axis and D is the nozzle exhaust diameter. These parameters were chosen to reproduce a realistic jet-wing configuration at the cutback take-off conditions. The axial distance between the nozzle exhaust and the plate trailing edge, denoted as L_{TE}, was varied in order to analyze four different conditions. Wall pressure fluctuations were measured both in the stream-wise direction, along the plate surface parallel to the jet centreline, and in the span-wise direction close to the trailing edge. The data were analyzed in order to provide an extensive statistical characterization that includes spectral quantities (auto-spectra and coherence), statistical moments and wavelet transform.

Details about the experimental setup are given in Sec. II and the results dealing with the pressure statistics are reported in Sec. III. Final conclusions are presented in Sec. IV.

Experimental setup

Measurements were performed in the ISVR Doak Laboratory at the University of Southampton where a $1/50^{th}$ model scale jet was installed. The ISVR Doak Laboratory is an anechoic chamber, fully anechoic above 400 Hz. The facility has dimensions approximately of 15 m-long, 7 m-wide and 5 m-high. The air jet is supplied by a high-pressure compressor reservoir system, with a maximum pressure of 20 Bar. Further details about the facility are reported in (14; 11). The experiment comprised an horizontal flat plate installed close to a single stream, unheated jet, under static ambient flow conditions. The jet diameter (D) measures 38.1 mm and the spreading half angle, evaluated via hot-wire measurement of the jet velocity field, is around 7° (11; 19). A 6 mm-thick, rectangular aluminium alloy flat plate was secured to a 2-axis traverse system so that it could be moved incrementally along (axially) or perpendicular (radially) to the jet axis. The total span of the plate was 1100 mm extending approximately $15D$ above and below the centreline of the jet. It was sufficiently large, therefore, to prevent the generation of additional noise from flow passing over the side edges. The total plate length L, or chord, of the plate was 762

mm, or $20D$. The leading edge of the plate was located upstream of the jet nozzle exit for all configurations, minimizing any acoustic leading edge effects. Thus, the plate is considered semi-infinite (i.e. leading edge and side-edge effects are negligible). The plate trailing edge was machined down (at an angle of $60°$) to a thickness of 1 mm. Figure 1 illustrates the experimental setup. The coordinate system has its origin at the nozzle exhaust, shown in white lines on the Figure 1.

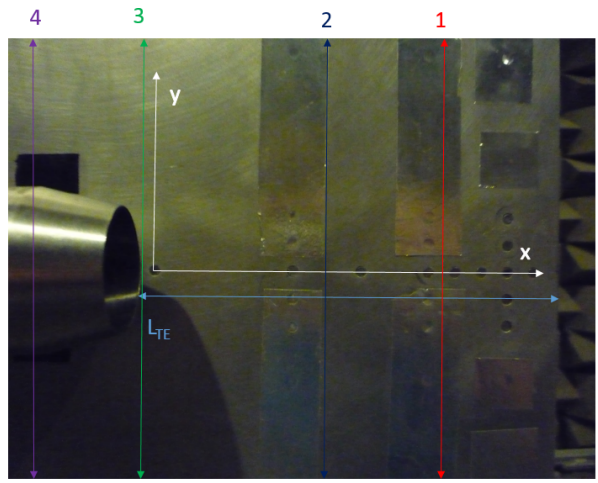

Figure 1. Experimental setup. Colored lines show the different nozzle exhaust positions from the TE: 1)$L_{TE}/D = 2$ in red line; 2) $L_{TE}/D = 4$ in blue line; 3)$L_{TE}/D = 7$ in green line; 4) $L_{TE}/D = 10$ in purple line

Wall pressure measurements were performed via flush mounted wall pressure transducers (Kulite Type XT-190) with a sensing diameter of 2 mm. The signals were acquired at a sampling frequency of 44 kHz and for a time of 10s. The investigations were performed at a radial position of the flat plate $H/D = 0.67$, measured from the jet geometric centreline to the surface of the plate. Four different configurations were analyzed varying the nozzle exhaust distance from the plate trailing edge (L_{TE}): $L_{TE}/D = 2$, $L_{TE}/D = 4$, $L_{TE}/D = 7$ and $L_{TE}/D = 10$.

The wall pressure measurement domain in the stream-wise direction varies from $x/D = -5$ up to $x/D = 10$ depending on the particular configuration. The span-wise pressure tappings were positioned close to the trailing edge and the measurement domain varied from $y/D = 0$ to

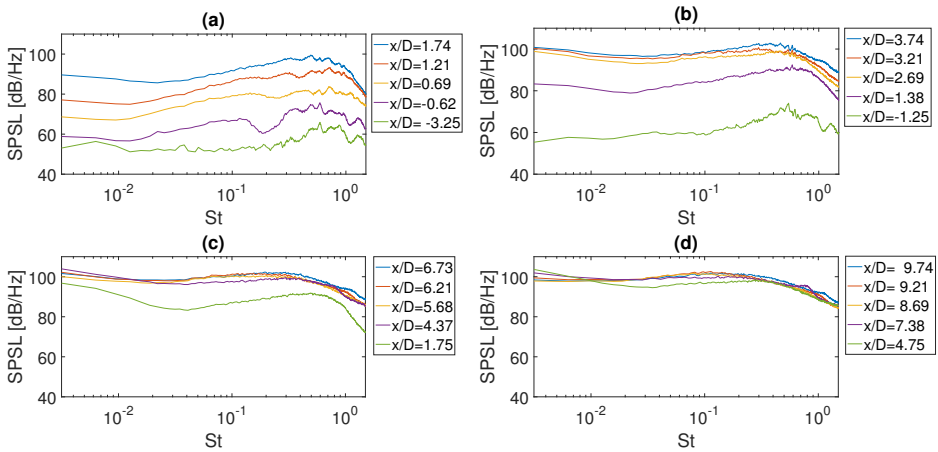

Figure 2. Wall pressure autospectra axial evolution for all the different configurations: (a) $L_{TE}/D = 2$; (b)$L_{TE}/D = 4$; (c) $L_{TE}/D = 7$; (d) $L_{TE}/D = 10$

$y/D = 2$. The axial spacing between the transducers was not constant. In the zone where the interaction between jet and plate was less, the transducers were positioned further apart compared to at the trailing edge. Similarly, in the span-wise direction, the distance between each pressure transducer increased as one moves farther from the jet centreline.

Results

The wall pressure fluctuations were analyzed in the frequency domain using the Sound Pressure Spectrum Level (SPSL) evaluated, according to (20), using the following equation:

$$SPSL = 10\log_{10}\left(\frac{PSD\Delta f}{P_{ref}^2}\right), \tag{1}$$

PSD is the power spectral density computed using the Welch method, $\Delta f = 1Hz$ is the frequency bandwidth and P_{ref} is the reference pressure equal to $20\mu Pa$. The SPSL is plotted versus the Strouhal number, defined as follows:

$$St = \frac{fD}{U_j}, \tag{2}$$

where U_j is the jet exit velocity.

In Figure 2, the axial evolution of the pressure autospectra is presented. The wall pressure transducer axial locations were, measured from the frame of reference fixed at the nozzle exhaust. In Figure 2(a), the first two spectra are acquired by pressure transducers mounted upstream of the nozzle exhaust. A series of peaks were detected over a range of Strouhal numbers that varies between $0.55 \leq St \leq 1.25$. This signature is also detectable in the first spectrum in Figure 2(b) related to an upstream transducers as well. As will be clarified later on, these peaks are signatures of upstream-travelling waves that become masked in the transducers locations downstream. Indeed, for the cases where the nozzle exhaust is positioned farther from the plate trailing edge, the spectra become more broadband taking on an universal trend similar of a boundary layer spectrum, as also shown in (17; 21). As an example, in Figure 2(d) the transducers are located more than $4D$ downstream of the nozzle, a region where a strong interaction exists between the jet and the plate surface. Consequently all of the pressure transducers sit within a turbulent boundary layer and the magnitude of the spectra, therefore, remain similar.

To gain a global point of view of the wall pressure fluctuation intensity over the plate surface for the different configurations, the Overall Sound Pressure Level (OASPL) was evaluated according to the following definition:

$$OASPL = 10 \log_{10} \left(\frac{\sigma_p^2}{P_{ref}^2} \right), \tag{3}$$

where σ_p is the standard deviation of the pressure signal (p). The OASPL trends for the different configurations are reported in Figure 3.

In agreement with the pressure autospectra, the OASPL energy content increases with increasing distance from the nozzle exit until the jet impact point is reached. The jet plate impact point is estimated using the jet spreading angle for the free jet case. Indeed, a constant trend of the OASPL is found in the configuration $L_{TE}/D = 10$ where a well developed turbulent boundary layer is formed on the plate. In the other three configurations, the OASPL rises consistently as the jet increasingly interacts with the surface. The minimum OASPL observed in the cases $L_{TE}/D = 2$ and 4 corresponds to transducers located upstream of the nozzle, a region where the jet's hydrodynamic pressure field weak. At large x/D the wall flow develops and the OASPL tends to reach the same amplitude independently of the distance from the leading edge.

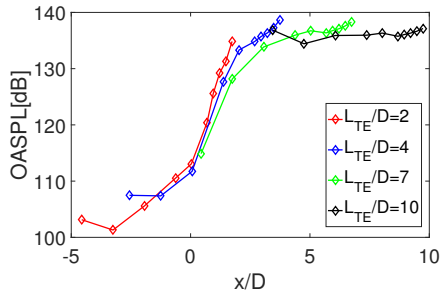

Figure 3. OASPL stream-wise evolution

In this region, the pressure fluctuations are probably dominated by the hydrodynamic component associated with the boundary layer vorticity.

This behavior is confirmed by analysis of high order statistical moments, namely skewness (s) and kurtosis (k), which are computed as follows:

$$s = \frac{E(p-\mu)^3}{\sigma_p^3}, \tag{4}$$

$$k = \frac{E(p-\mu)^4}{\sigma_p^4}, \tag{5}$$

where μ is the mean of the signal p and E( ) is the expected value. As shown in Figure 4(a), the skewness factor evolution along the plate varies consistently in the four cases. A zero skewness is achieved along a large spatial region and a positive bump is achieved in the position close to the impact point. Johansson et al. (22), Dhanak et al. (23) and Camussi et al. (24) associated positive and negative pressure events educed in fully developed TBL to inward and outward (or ejections, see also (25)) motions respectively. The positive Skewness observed in our results can then be ascribed to the prominence of inward events induced by the impact of the jet vortical structures on the plate. Upstream of the impact point the symmetric statistics reappear as an effect of a statistical homogenization of the turbulent flow.

The kurtosis trend reported in Figure 2(b), qualitatively follows the OASPL evolution of Figure 3. Kurtosis values close to three are detected for the kulites positioned upstream of the nozzle exhaust, thus in an acoustic near field and not influenced by jet turbulent structures.

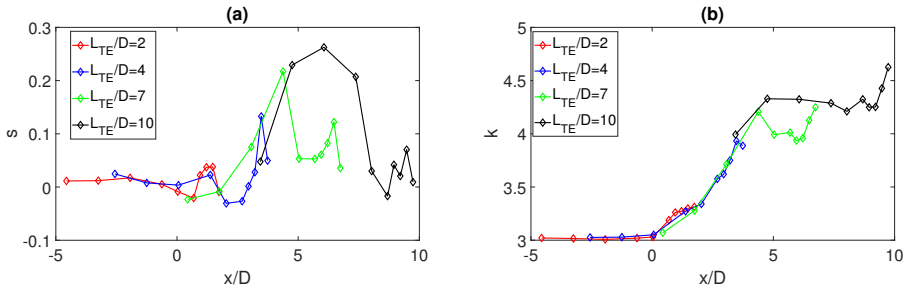

Figure 4. (a)Skewness stream-wise evolution. (b)Kurtosis stream-wise evolution

Furthermore the variation of the plate trailing edge from the nozzle exhaust does not make a detectable effect on the upstream kurtosis values. While going downstream, the development of the boundary layer over the plate is characterized by an increase in intermittency, typical of turbulent flows, which is seen in the regions where the kurtosis is larger than 3.

The two point statistics of the jet induced wall pressure fluctuations have been investigated in the time domain via the cross correlation function computed between two contiguous pressure transducers. The cross-correlation is defined as

$$R_{pp} = E[p(x,t), p(x+\xi, t+\tau)], \tag{6}$$

where ξ is the distance in the stream-wise direction between the two transducers, τ is the time lag and the symbol $<>$ denotes a time average. The cross-correlations coefficients ρ_{pp}, obtained normalizing R_{pp} by the product of the standard deviations of the two pressure signals, are plotted in Figure 5 for the four jet-plate configurations and a few reference positions

It is interesting to note that for the configurations $L_{TE}/D = 2$ and 4, the maximum correlation between pressure transducers positioned upstream of the nozzle exhaust occurs at a negative time delay thus evidencing the signature of perturbations travelling upstream. This behaviour is accompanied by an increase in magnitude of the oscillations probably related to the peaks observed in the auto-spectra in Figure 2a. Similar results are also shown in a small scale jet wing flap configuration (5). In the cases (c) and (d) the oscillations disappear and the peak is at positive time delays. For increasing x/D the cross-correlation coefficients tend to

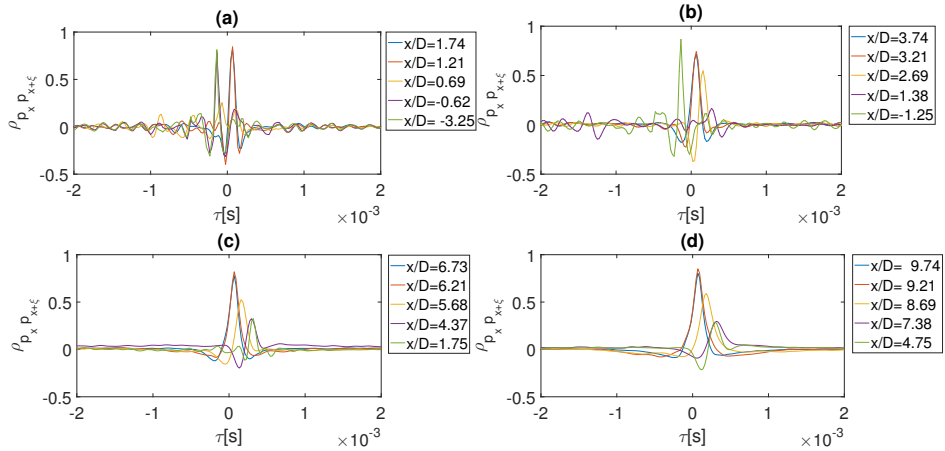

Figure 5. Wall pressure stream-wise cross-correlations for all the different configurations: (a) $L_{TE}/D = 2$; (b)$L_{TE}/D = 4$; (c) $L_{TE}/D = 7$; (d) $L_{TE}/D = 10$. Axial positions in figure legends refer to the first of two consecutive pressure transducers.

broaden describing the large scale turbulent structures induced by the jet (17).

The time lag τ at which the cross-correlation peak is located, and the separation between the transducers ξ, can be combined to compute the stream-wise phase velocity $U_p = \frac{\xi}{\tau}$ as reported in Figure 6 for the different configurations. According to the above discussion, a negative phase velocity is found for the transducers positioned upstream of the nozzle exhaust. The absolute amplitude is close to the speed of sound confirming that in this region acoustic waves propagates upstream and the hydrodynamic pressure is negligible. At larger x/D, the phase velocity is positive and with a magnitude that is about 70% of the jet velocity, thus much lower than the speed of sound. This behaviour reflects the hydrodynamic convection that becomes dominant in all the considered configurations for $x/D > 0$.

The two point statistics are further explored in the frequency domain by the computation of the spectral coherence function evaluated as follows (26):

$$\gamma(\xi, \eta, \omega) = \frac{|CPSD_{p_1 p_2}(\xi, \eta, \omega)|}{[PSD_{p_1}(\omega) PSD_{p_2}(\omega)]^{\frac{1}{2}}}, \tag{7}$$

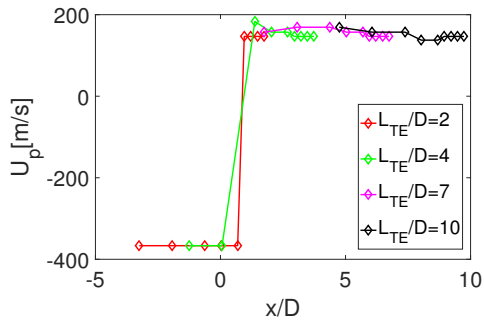

Figure 6. Axial evolution of the phase velocity

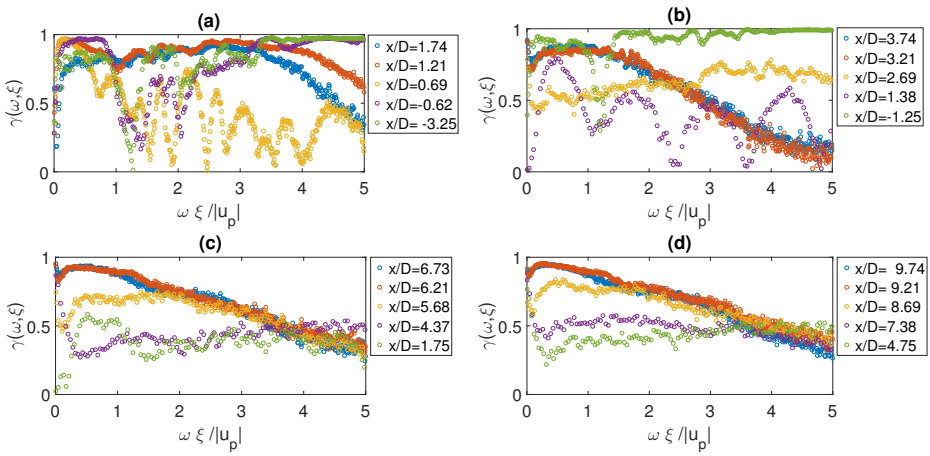

Figure 7. Wall pressure stream-wise coherences for all the different configurations: (a) $L_{TE}/D = 2$; (b)$L_{TE}/D = 4$; (c) $L_{TE}/D = 7$; (d) $L_{TE}/D = 10$. Axial positions in figure legends refer to the first of two consecutive pressure transducers.

where ω is the angular frequency, $CPSD_{p_1p_2}$ is the cross-spectrum, and $PSD_{p_1}$and PSD_{p_2} are the auto-spectra of two consecutive transducers separated in the stream-wise direction by ξ and in the span-wise direction by η.

The coherence spectra computed for stream-wise separations as functions of the normalized angular frequency $\omega\xi/U_p$ are shown in Figure 7. According to literature, in the case of fully developed TBL, an exponential decay of the coherence function is expected. In the present

cases, an exponential-like decay is observed for the cases $L_{TE} > 2$ (Figure 7b, c, d) and for the largest x/D. In the other cases, corresponding to transducers positioned upstream of or close to the nozzle exhaust, a flat or oscillatory trend is observed. This is an indication of the absence of hydrodynamic fluctuations which become relevant only downstream of the nozzle exhaust.

A similar trend is observed in the span-wise direction. The coherence function $\gamma(\omega, \eta)$ is computed considering the transducers close to the trailing edge separated by the distance η in the span-wise direction. Examples are reported in Figure 8 and, according to the above discussion, the region where exponential-like decay is observed corresponds to $L_{TE} > 2$ (Figure 8 b, c, d). In terms of y/D, the exponential decay is observed for transducers located close to $y/D = 0$. In this area, the jet flow interacts with the plate and induces a strong hydrodynamic pressure. According to literature, the coherence decay in the span-wise direction is seen to be faster than in the stream-wise direction. Moreover, a higher coherence is detected for the farther span-wise Kulites positions from the jet axis The working hypothesis is the lower jet-plate interaction present in these positions, which probably reduces the jet induced turbulent boundary layer over the plate surface

It can be concluded that, according to previous studies on an infinite flat plate ((8; 17)), in the region where the jet flow interacts with the plate, theoretical models proposed for canonical TBL to predict the coherence decay can be applied successfully. As a reference example, the Corcos' model (27) can be considered. This approach predicts a purely exponential decay of the coherence function according to the following formulation,

$$\gamma(\xi, \eta, \omega) = e^{-\alpha \frac{\omega \xi}{U_c}} \cdot e^{-\beta \frac{\omega \eta}{U_c}} \cdot e^{i \frac{\omega \xi}{U_c}}. \tag{8}$$

The first two exponential terms refer to the stream-wise and span-wise wall pressure coherence length respectively and the last exponential term accounts for the mean pressure field. Taking into account the fact that the coherence decay takes on an exponential form only where a turbulent boundary layer exists, a comparison against the Corcos' fit is made using the experimental data at the trailing edge for the configuration $L_{TE}/D = 10$. An example is reported in Figure 9 showing that the experimental stream-wise coherence is well reproduced by the exponential

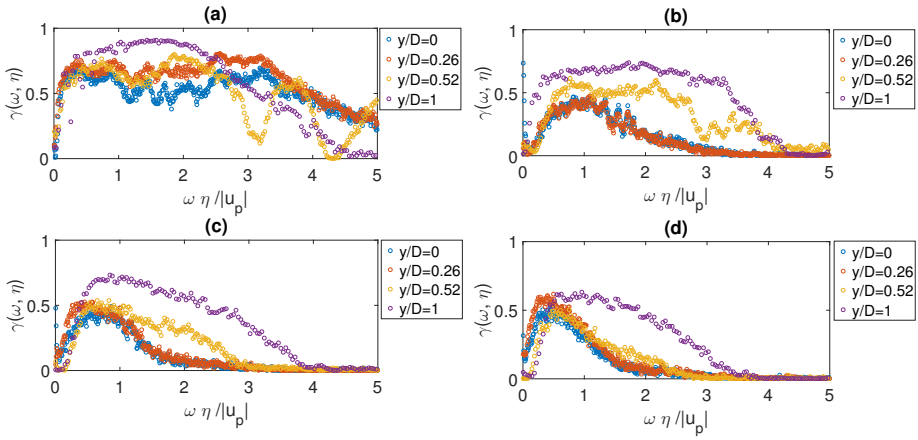

Figure 8. Wall pressure span-wise coherences for all the different configurations: (a) $L_{TE}/D = 2$; (b)$L_{TE}/D = 4$; (c) $L_{TE}/D = 7$; (d) $L_{TE}/D = 10$. Axial positions in figure legends refer to the first of two consecutive pressure transducers.

law computed with Corcos' exponent. The discrepancies are may be due to the additional vorticity generated by the TE.

For modelling purposes, another important quantity that can be obtained from the span-wise coherence is the span-wise correlation length whose definition is as follows:

$$\lambda_\eta(\omega) = \int_0^\infty \gamma^2(\omega, \eta) d\eta \tag{9}$$

This quantity is important as it is the input of analytical models able to predict the sound scattered to the far field (28). Figure 10 shows the correlation lengths in the span-wise direction for all the different studied configurations. Apart for $L_{TE}/D = 2$, where a TBL is not seen at the TE, the others cases show a consistent trend with regards to the loss of high frequency coherence due to the development of a turbulent boundary layer as a result of the interaction between the jet stream and the plate.

The consistent decrease of the coherence length scale with plate length may suggest that the a very small turbulent boundary layer increases with L/D. To make this assertion more robust, further investigations are necessary.

In order to further describe the statical properties of the pressure fluctuations, a time-frequency investigation is carried out by application

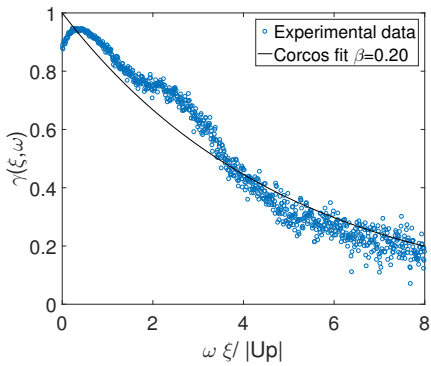

Figure 9. Comparison between experimental data and Corcos' fit at x/D=9.21 and $L_{TE}/D = 10$

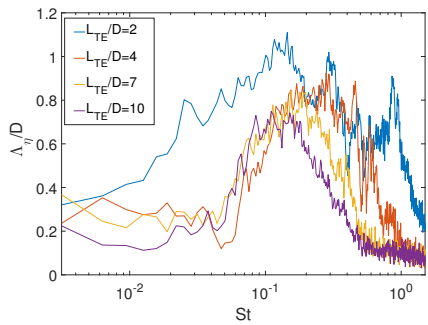

Figure 10. Span-wise integral coherence lengths

of the continuous wavelet transform (CWT). The CWT consists of a projection of a given signal over a basis of compact support functions obtained by the translation and dilatation of a so-called mother wavelet. The wavelet transform can be formalized as follows(29; 18):

$$w(s,t) = C_{\psi}^{\frac{-1}{2}} \int_{-\infty}^{\infty} p(\tau)\psi^*\Big(\frac{t-\tau}{s}\Big), \tag{10}$$

where s is the scale dilatation parameter corresponding to the width of the wavelet, τ is the translation parameter corresponding to the position of the wavelet, $C_{\psi}^{\frac{-1}{2}}$ is a coefficient that takes into account the mean value of

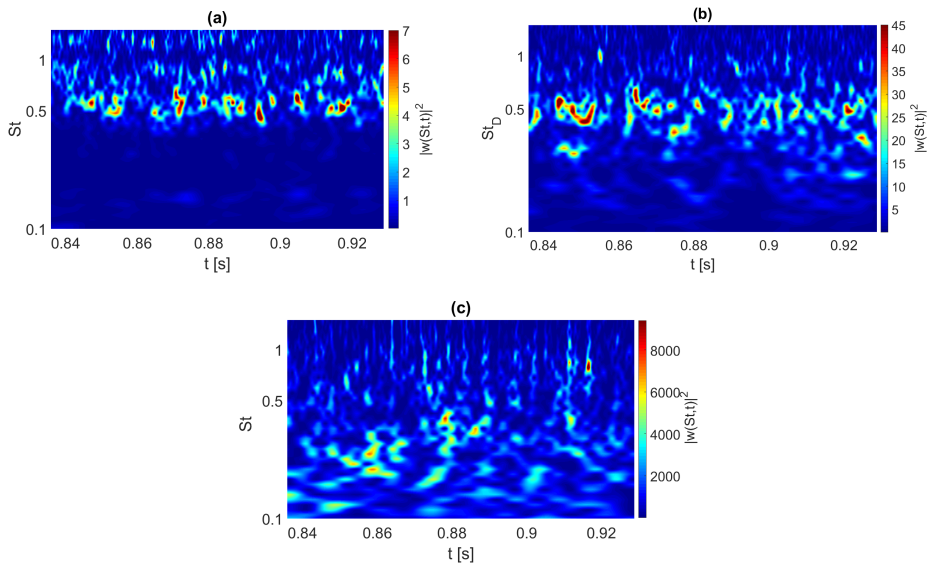

Figure 11. Wavelet scalograms:(a) $L_{TE}/D = 2$ and x/D=-3.25; (b) $L_{TE}/D = 4$ and x/D=4.37;(c) $L_{TE}/D = 10$ and x/D=9.21

$\psi(t)$ and $\psi^*\left(\frac{t-\tau}{s}\right)$ is the complex conjugate of the dilated and translated mother wavelet $\psi(t)$. The kernel selected is the $Bump$ wavelet(30; 29) with the pulsation of the unit scale wavelet spectrum set at $\mu = 5$ and the wavelet width at $\sigma = 0.6$.

Figure 11 reports examples of the time-frequency representation of the wavelet scalogram obtained by the square of the wavelet coefficients. The signal taken at $x/D = -3.25$ in the configuration $L_{TE}/D = 2$, is reported in Figure 11(a). The time-frequency representation clearly evidences the presence of localized high energetic bumps. According to the interpretations given above, the energy contained in the interval $0.55 \leq St \leq 1.27$ is related to upstream travelling waves. The time-frequency analysis highlights that these modes are not active continuously but they, even though well localized in terms of St, appear randomly in time. Considering pressure transducers downstream of the nozzle exhaust (Figure 11b), the energy amplitude increases significantly and the most energetic signatures move towards lower frequencies. As clarified above, downstream of the nozzle exhaust the hydrodynamic, pressure dominates and the observed signatures, concentrated within the range $0.3 \leq St \leq$

0.8, may be interpreted as a trace of the jet Kelvin-Helmholtz instability. According to (31) and (32) the energy associated with the Kelvin-Helmholtz mode is characterized by an intermittent statistics revealed again by the random nature of the energetic bumps.

Figure 11(c) corresponds to a transducer located close to the trailing edge in the configuration $L_{TE}/D = 10$. In this case, according to the analyses presented above, the flow is fully developed and the energetic events are randomly distributed both in the time and frequency domains.

Conclusions

An experimental study has been carried out to investigate the interaction between a subsonic single stream compressible jet and a semi-finite flat plate parallel to the jet axis. The plate is installed very close to the jet in order to be representative of a scaled modern aircraft jet-wing configuration. The focus of this work in on the wall pressure fluctuations induced by the jet over the plate surface and the dependency of their statistics on the axial distance between the jet nozzle and the plate trailing edge. For this purpose, the radial jet-plate separation is kept constant and four different axial distances L_{TE} of the nozzle exhaust from the plate trailing edge are considered.

The investigation was performed in an anechoic environment using an array of flush mounted wall pressure transducers positioned in the stream-wise direction along the jet axis and in the span-wise direction close to the plate trailing edge.

The analyses in the Fourier and physical domains shows the relevant influence of the parameter L_{TE}/D. The region upstream of the jet exhaust is characterized by the presence of upstream travelling waves whose trace has been identified both in the auto-spectra and cross-correlations. The upstream modes are characterized by a negative propagation velocity close to the speed of sound. In this region the statistics are almost Gaussian and the OASPL is relatively low.

An intermediate region is then identified close to the point where the jet flow impacts the plate. The OASPL increases and the statistics becomes strongly non-Gaussian. In the positions downstream of the jet nozzle exit, but upstream of the impact point, the trace of the Kelvin-Helmholtz instability is apparently observed as well.

Further downstream and for increasing L_{TE}/D the flow rapidly evolves towards a quasi developed state and the statistical properties become similar to those commonly observed in turbulent boundary layers. This region is dominated by hydrodynamic pressure fluctuations characterized by a constant positive propagation velocity that, as expected, is a fraction of the speed of the jet stream. The statistics are seen to become intermittent and the OASPL remains about constant. In this region, the coherence function decays exponentially and the classical Corcos model applies reasonably well. Furthermore, the span-wise coherence length has a shape similar to that achieved in fully developed boundary layers. This result is important for the prediction of far field trailing edge noise.

Analysis of the wavelet scalogram in the time-frequency domain shows that, in the region where the jet interacts with the plate, a random distribution of energy events is detected both in time and frequency. This is in agreement with the broadband nature of the Fourier spectra observed at these positions. In the other regions on the plate, it is observed that both the upstream and the downstream travelling modes, even though localized in terms of frequency, are intermittent in their temporal evolution. Energy bumps are indeed seen to appear at about constant frequency but randomly in time.

References

[1] Lighthill M. J. 1952 On sound generated aerodynamically. I. General theory. Proc. R. Soc. Lond. A 211 (1107), 564–587.

[2] Huber J., Jordan P., Roger M., Gervais Y., Lizarazu D., Wlassow F., (2017) Exploring Flight Effects for Installed Jet Noise using Wavepacket Sound-Source Model. AIAA paper 2017-3382. 23nd AIAA/CEAS Aeroacoustics Conference Denver, Colorado, USA

[3] Huber J., Drochony G., Pintado-Peno A., Cléro F. Bodard G. Large-Scale Jet Noise Testing, Reduction and Methods Validation "EXEJET": 1. Project Overview and Focus on Installation. 20th AIAA/CEAS Aeroacoustics Conference, AIAA AVIATION Forum, AIAA 2014-3032. https://doi.org/10.2514/6.2014-3032

[4] Lawrence J. Self R.H. (2015) Installed jet-flap impingement tonal noise. 21st AIAA/CEAS Aeroacoustics Conference. AIAA 2015-3118. https://doi.org/10.2514/6.2015-3118

[5] Meloni S., Mancinelli M., Camussi R., and Huber J. (2020) Wall-Pressure Fluctuations Induced by a Compressible Jet in Installed Configuration. AIAA Journal. https ://doi.org/10.2514/1.J058791

[6] Michel U., Kramer F., Mockett C., (2019)The dominating influence of large-scale jet motion on jet-wing interaction noise. AIAA paper 2019-2431 25nd AIAA/CEAS Aeroacoustics Conference Delft, The Netherlands. https://doi.org/10.2514/6.2019-2431

[7] Tyacke J.C., Wang Z.N., Tucker P.G. (2019). LES–RANS of Installed Ultra-High-Bypass-Ratio Coaxial Jet Aeroacoustics with Flight Stream. AIAA Journal, 1–22. doi:10.2514/1.j057057

[8] Di Marco A., Mancinelli M., Camussi R. (2015) Pressure and velocity measurements of an incompressible moderate Reynolds number Jet interaction with a tangential flat plate. Journal of Fluid Mechanics 770:247-272. https://doi.org/10.1017/jfm.2015.149

[9] Mancinelli M., Camussi R. (2018) Acceleration and wall pressure fluctuations generated by an incompressible jet in installed configuration. Comptes Rendus Mécanique, 346:10, 919-931, https://doi.org/10.1016/j.crme.2018.07.008

[10] Meloni S., Di Marco A., de Paola E., Camussi R., Fava G.(2019) Pressure and Velocity Measurements of a Compressible Jet Interacting with a Flat Plate. Progress in Turbulence VIII, Springer Proceedings in Physics 226,https://doi.org/10.1007/978-3-030-22196-643

[11] Proença A. (2018) Aeroacoustics of isolated and installed jets under static and in-flight conditions. PhD thesis

[12] Cavalieri A.V.G., Jordan P., Wolf W.R., Gervais Y., (2014) Scattering of wavepackets by a flat plate in the vicinity of a turbulent jet. Journal of Sound and Vibration, 333:6516-6531. https://doi.org/10.1016/j.jsv.2014.07.029

[13] Papamoschou D. , Mayorlal S. (2009) Experiments on shielding of jet noise by airframe surfaces. AIAA Paper2009-3326. https://doi.org/10.2514/6.2009-3326

[14] Lawrence J., Azarpeyvand M., Self R.H., (2011) Interaction between a Flat Plate and a Circular Subsonic Jet . 17th AIAA/CEAS Aeroacoustics Conference (32nd AIAA Aeroacoustics Conference) Portland, Oregon. https://doi.org/10.2514/6.2011-2745

[15] Mancinelli M. ,Di Marco A., Camussi R. (2017) Multivariate and conditioned statistics of velocity and wall pressure fluctuations induced by a jet interacting with a flat plate.Journal of Fluid Mechanics 823:134-165. https://doi.org/10.1017/jfm.2017.307

[16] Meloni S., Di Marco A., Mancinelli M., Camussi R.(2018) Reynolds numbers effect on wall pressure fluctuations induced by a subsonic jet on a tangential flat plate. FIV2018 (Toronto).

[17] Meloni S., Di Marco A., Mancinelli M., Camussi R.(2019) Wall pressure fluctuations induced by a compressible jet flow over a flat plate at different Mach numbers. Exp Fluids 60: 48. https://doi.org/10.1007/s00348-019-2696-3

[18] Meloni S., Di Marco A., Camussi R. , Mancinelli M. (2019) Parametric characterization of wall pressure fluctuations induced by a compressible jet flow interacting with a flat plate 25th AIAA/CEAS Aeroacoustics Conference AIAA 2019-2711 Delft, The Netherlands https://doi.org/10.251

[19] Proença A., Lawrence J., Self R.H. Measurements of the single-point and joint turbulence statistics of high subsonic jets using hot-wire anemometry. Exp Fluids (2019) 60: 63. https://doi.org/10.1007/s00348-019-2716-3

[20] Pierce A.D. 1981 Acoustics: An Introduction to its Physical Principles and Applications. McGraw-Hill

[21] Farabee M., Casarella M.J. (1991) Spectral features of wall pressure fluctuations beneath turbulent boundary layers . Physics of Fluids Dynamics 3. https://doi.org/10.1063/1.858179

[22] Johansson A. V., Her J.Y., Haritonidis J. H., (1987) On the generation of high-amplitude wall-pressure peaks in turbulent boundary layers and spots. Journal of Fluid Mechanics, 175, 119-142. doi:10.1017/S0022112087000326

[23] Dhanak, M.R. and Dowling, A.P. and S. C (1997) Coherent vortex model for surface pressure fluctuations induced by the wall region of a turbulent boundary layer. PHYS FLUIDS, 9. pp. 2716-2731. ISSN 1070-6631

[24] Camussi, R., Robert, G., Jacob, M. (2008). Cross-wavelet analysis of wall pressure fluctuations beneath incompressible turbulent boundary layers. Journal of Fluid Mechanics, 617, 11-30. doi:10.1017/S002211200800373X

[25] Jayasundera, S., Casarella, M. Russel, S. 1996 Identification of coherent motions using wall pressure signatures. Tech. Rep. 19960918-036, Catholic Univ. of America, Washington DC. (available at http://handle.dtic.mil/100.2/ADA314537)

[26] Di Marco A., Camussi R., Bernardini M., Pirozzoli S. (2013). Wall pressure coherence in supersonic turbulent boundary layers. Journal of Fluid Mechanics, 732, 445-456. doi:10.1017/jfm.2013.410

[27] Corcos G.M. (1964) The structure of the turbulent pressure field in boundary-layer flows. Journal of Fluid Mechanics 18:353-378

[28] Amiet R.K. (1976) .Noise due to turbulent flow past a trailing edge. Journal of Sound and Vibration. 46:3 387-393 $https://doi.org/10.1016/0022-460X(76)90948-2$

[29] Mancinelli M., Jaunet V., Jordan P., Towne A. (2019) Screech-tone prediction using upstream-travelling jet modes Exp Fluids 60: 22. https://doi.org/10.1007/s00348-018-2673-2

[30] Jordan P., Jaune V.,Towne A., Cavalieri A., Colonius T.,Schmidt O., Agarwal A. (2018) . Jet–flap interaction tones. Journal of Fluid Mechanics 853:333-358 https://doi.org/10.1017/jfm.2018.566

[31] Camussi R.,Di Marco A., Castelain T.,(2017) Statistical analysis of the hydrodynamic pressure in the near field of compressible jets. International Journal of Heat and Fluid Flow. 64:1-9.https://doi.org/10.1016/j.ijheatfluidflow.2017.01.007

[32] Camussi R, Mancinelli M., Di Marco A. (2017)Intermittency and stochastic modeling of hydrodynamic pressure fluctuations in the near field of compressible jet. International Journal of Heat and Fluid Flow. 68:180-188. https://doi.org/10.1016/j.ijheatfluidflow.2017.10.008.